Additive Manufacturing 60 (2022) 103204

Contents lists available at ScienceDirect

Additive Manufacturing

journal homepage: www.elsevier.com/locate/addma

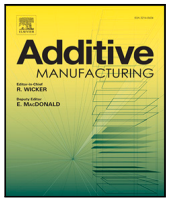

Research paper

Influence of laser shock peening on the residual stresses in additively manufactured 316L by Laser Powder Bed Fusion: A combined experimental–numerical study

Paul Sandmann [a,*], Sören Keller [b], Nikolai Kashaev [b], Shaaz Ghouse [a], Paul A. Hooper [a], Benjamin Klusemann [b,c], Catrin M. Davies [a]

[a] Department of Mechanical Engineering, Imperial College London, Exhibition Road, London SW7 2AZ, UK
[b] Institute of Materials Mechanics, Helmholtz-Zentrum Hereon, Max–Planck-Straße 1, 21502 Geesthacht, Germany
[c] Institute of Product and Process Innovation, Leuphana University of Lüneburg, Universitätsallee 1, 21335 Lüneburg, Germany

ARTICLE INFO

Keywords:
Laser shock peening
Laser powder bed fusion
LPBF 316L stainless steel
Residual stress
Finite element analysis
Additive manufacturing

ABSTRACT

Detrimental subsurface tensile residual stresses occur in laser powder bed fusion (LPBF) due to significant temperature gradients during the process. Besides heat treatments, laser shock peening (LSP) is a promising technology for tailoring residual stress profiles of additively manufactured components. A multi step process simulation is applied aiming at predicting the residual stress state after applying LSP to a cuboid shaped specimen manufactured by LPBF in two different building directions as well as comparing it with a post-build heat treatment. The validity of the numerical simulation is evaluated based on comparisons of residual stresses determined by incremental hole drilling technique within different stages of the multi step process: in the as-build condition, after subsequent heat treatment as well as after applying LSP to the as-build and heat treated specimens, showing overall a good experimental–numerical agreement throughout each of the process stages. Applying a heat treatment to the as-build LPBF sample at 700 °C for 6 h showed not to be effective in eliminating the surface tensile stress entirely, reducing the tensile residual stresses by 40%. However, the application of LSP on LPBF components showed promising results: LSP was able even to convert the detrimental near surface tensile residual stresses in the LPBF component into compressive residual stresses next to the surface, which is known to be beneficial for the fatigue performance.

1. Introduction

Additive manufacturing (AM) processes such as laser powder bed fusion (LPBF) allow the production of component geometries which are difficult or even impossible to produce using conventional manufacturing processes. LPBF is a powder bed fusion technology whereby the powder bed in the chamber is exposed to a laser beam with a high energy density heat flux, causing the powder to fully melt and solidify upon cooling [1]. The process is capable of producing parts with near full density and mechanical properties comparable to bulk materials or even better as shown by Kruth et al. [2].

Despite microstructural material defects such as lack-of-fusion, gas and keyhole porosity, in additive manufacturing processes [3], excessive residual stresses are often reported close to the materials yield strength due to uneven heat input and rapid cooling [4,5]. This not only reduces the geometrical accuracy of the component [6] but also affects the material properties. McClung [7] has shown that the presence of large residual stresses can especially alter the mechanical response in cyclic loading and affect the fatigue performance.

In order to predict residual stresses in a structural components, Finite Element (FE) simulations have been shown to be very suitable. However, since LPBF consists of several hundred or even thousand individually melted layers that are only 20-100 μm thick, the direct modelling of the process via a coupled thermo-mechanical simulation demands enormous computational cost. Therefore, most often a sequentially coupled thermo-mechanical analysis is performed, i.e. a transient heat transfer analysis is performed first, sequentially coupled to the mechanical analysis [9]. Great efforts have been made by Hussein et al. [10] and Parry et al. [11] to understand the modelling of a single layer or a single scan track in LPBF to get insight into the effect of the scan strategy, laser power and laser speed on the residual stresses. However, multi-layer effects leading to residual stresses developing in the building direction, are neglected using this approach. Hence Williams et al.

* Corresponding author.
E-mail address: paul.sandmann18@imperial.ac.uk (P. Sandmann).

https://doi.org/10.1016/j.addma.2022.103204
Received 6 July 2022; Received in revised form 3 October 2022; Accepted 7 October 2022
Available online 13 October 2022

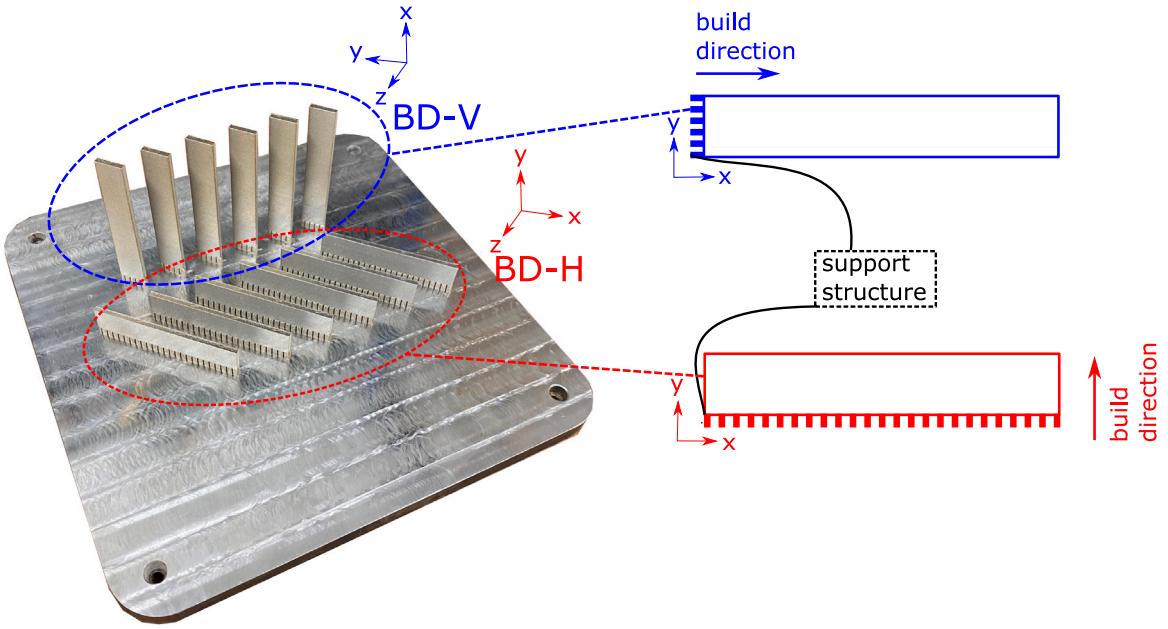

Fig. 1. Arrangement of the investigated geometry on the build plate: 6 horizontal (BD-H) and 6 vertical (BD-V) specimen were manufactured using a stripe scanning strategy [8] with 67° degree rotation between each layer via the Renishaw AM250 LPBF machine. The coordinate system is defined based on the sample geometry and not the build plate.

[12] developed a strategy to reduce the computational effort while modelling full components by grouping a large number of thin layers to bigger layers in the simulation, while remaining reasonable accuracy.

After all, there are effective post-processing methods to mitigate or modify the high tensile stresses initially present in LPBF parts. Stress relieving post-build heat treatment is the most common approach as explored by Williams et al. [4] and Shiomi et al. [13]. Shiomi et al. [13] showed for a chrome molybdenum steel (JIS SCM440) that annealing can reduce the residual stresses by up to 70%, however, dissolving the beneficial cellular dendritic structure responsible for the high yield strength and excellent ductility of the build. In contrast, Williams et al. [4] performed post-build heat-treatment of 316l stainless steel for 2 h at 650 °C, showing only a minor stress relieving effect.

Another promising approach to tailor residual stresses is laser shock peening (LSP). Kalentics et al. [14] developed a hybrid process applying LSP during different layers of the LPBF process and showing that tensile stresses can be converted into compressive close to the surface. As a result of the tailored residual stress profile, fatigue properties improved for materials manufactured by 3D-LSP as shown by Kalentics et al. [15]. Hybrid 3D-LSP also showed to improve the geometrical accuracy [16]. Lastly, Kalentics et al. [17] reveals that the hybrid LSP process can heal cracks for alloys that are sensitive to cracking.

Generally, all peening processes rely on the principle of inducing compressive residual stresses near the surface to prevent or inhibit crack propagation Zhang et al. [18], which should lead to an increase in the fatigue life which has already been demonstrated for additive manufactured samples by Hackel et al. [19]. The idea of applying LSP to an LPBF component is to convert detrimental near surface tensile residual stresses observed in the as-build condition to beneficial compressive residual stresses, where compressive stresses induced by LSP can reach well above 1 mm depth [20].

This paper presents a combined experimental–numerical approach, investigating the residual stresses at various stages of LSP post-processed and heat treated LPBF components. To be able to tailor the residual stresses in LPBF components with the help of LSP, a multi-step simulation approach is developed. For this purpose, the process simulations of the different processes are sequentially coupled. At first, a LPBF process simulation is used to predict the initial residual stresses after the build followed by an optional visco step to take potential heat treatments into consideration. Subsequently, the near surface residual stress state is modified via simulating the LSP process, providing the final residual stress state of the LSP post-process LPBF structure.

2. Experimental procedures

2.1. Laser powder bed fusion

In the present study cuboid shaped bars (77 mm × 13.5 mm × 3 mm) were investigated, as depicted in Fig. 1. All specimens were manufactured from 316L stainless steel with a Renishaw AM250 LPBF machine on a 5 mm support structure using a stripe scanning strategy [8] with 67° degree rotation between each layer. The arrangement of the cuboid shaped bar on the build plate is shown in Fig. 1. All samples were removed from the build plate at the support structure using a hacksaw. The LPBF process parameters employed are the same for all investigated samples as summarized in Table 1. The composition of the used 316L powder is given in Table 2. No preheating of the build plate was used in the present study. The temperatures of a thermocouple in the build plate recorded temperatures with a maximum of 43 °C during the LPBF process.

2.2. Laser shock peening

The LSP process is illustrated in Fig. 2. The surface of the material is irradiated with a short duration laser pulse to vaporize material close to the surface. The ionization of atoms leads to the generation of plasma which is rapidly expanding [20], resulting in a pressure pulse acting on the surface. This pressure pulse introduces mechanical shock waves causing local plastic deformation within the material, which subsequently lead to the formation of compressive residual stresses after relaxation of the system [22].

LSP was performed with an Nd:YAG laser (wavelength 1064 nm) and a squared focus, i.e. 1 mm or 3 mm, respectively. The laser pulse energy was varied between 3 to 5 J, the Gaussian-shaped pulse profile had a Full Width at Half Maximum (FWHM) of 20 ns and the laser frequency was set to 10 Hz. The selected focus size and peening energy amount to a laser power density of 2.78 GW/cm^2 and 25 GW/cm^2 at a laser energy of 5 J for the 3 mm×3 mm and 1 mm×1 mm focus size, respectively. A laminar water film is applied on the specimen surface

Table 1
LPBF parameters employed.

Laser power [W]	Exposure time [µs]	Point distance [µm]	Layer thickness [µm]	Hatch spacing [µm]	Powder size [µm]	Incremental angle [°]
200	80	40	50	110	10	67

Table 2
Composition of stainless steel 316L-0407 metal powder for additive manufacturing [21].

Composition	C	Mn	P	S	Cr	Mo	Ni	O	N	Fe
wt.%	<0.03	<2	<0.045	<0.03	16–18	2–3	10–14	<0.1	<0.1	balance

Table 3
Hole drilling increments selected for the in-depth measurement. Due to an expected higher stress gradient at the surface, smaller increments are followed by bigger increments deeper in the material.

Increment [–]	1	2	3	4	5	6	7	8	9	10	11	12	13	14
Depth [mm]	0.025	0.05	0.1	0.15	0.2	0.25	0.3	0.4	0.5	0.6	0.7	0.8	0.9	1

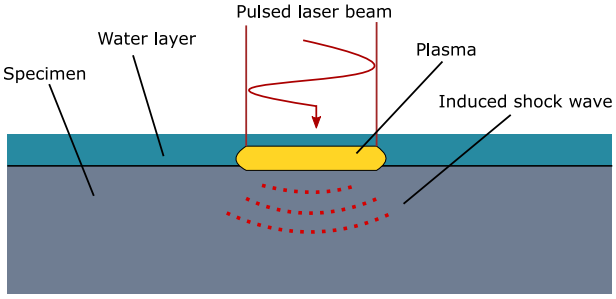

Fig. 2. Schematic of the LSP process. The laser pulse induces a shock wave by vaporization material close to the surface and forming a rapidly expanding plasma. This shock wave leads to local plastic deformation and ultimately compressive residual stresses below the surface.

during peening, increasing the efficiency due to an increased duration and maximum of the plasma pressure. No additional sacrificial overlay was used during the LSP experiments. The laser is fixed in position and the sample is moved by a robot for each respective peening pulse. An area of 30 mm × 13.5 mm of the additively manufactured bars has been peened with an overlap of 30% in x and y direction covering the entire height of the part (see Fig. 3). The peening pattern has been kept identical for all samples with respect to the samples geometry and for some samples a sequence overlap has been performed. The LSP advancing direction is parallel to the LPBF build direction for the vertical samples (LPBF BD-V) and perpendicular to the LSP advancing direction for the horizontal samples (LPBF BD-V) as schematically shown in Fig. 3.

2.3. Post-build heat treatment

After sectioning the samples from the build plate, a heat treatment in a standard furnace for 6 h at 700 °C was applied. The samples were left in the furnace for 48 h to cool down after the heat treatment achieving a slow cooling rate and therefore minimize through-wall temperature gradients to ensure no additional thermal stresses are reintroduced. Previous studies have revealed that beyond a temperature of 700 °C, the cellular dendritic structure and the melt pool boundaries are dissolving in LPBF 316L as shown by Montero Sistiaga et al. [23]. Thus, a heat treatment temperature leaving the microstructure unaffected was chosen, aiming at preserving the yield stress of the as-build condition while reducing the residual stresses sufficiently [24].

2.4. Residual stress analysis via incremental hole drilling method

Residual stresses were determined using the hole drilling system PRISM from Stresstech. The system utilizes electronic speckle interferometry (ESPI) to determine surface deformations. The process can be subdivided into three steps as described by [25]:

1. Drilling a hole in the specimen incrementally.
2. Measuring the resulting surface deformation after each increment.
3. Calculate (Integral method) the corresponding residual stress from the surface deformation.

After each drilling increment, the specimen is illuminated with coherent light (laser beam). The natural roughness leads to diffused light scatter, which is visible on the image captured by a Charge-Coupled Device (CCD) camera as light and dark speckles (speckle pattern). The sample surface deforms due to the stress relaxation occurring for each drilling increment when material is removed that contained residual stresses. This displacement can be quantified by imaging the speckle pattern before and after the surface deformation [26]. Subsequently, the integral method is applied to calculate the residual stresses from the measured deformation based on elastic finite element calculations and solved by a full field least square technique, as described by Ponslet and Steinzig [27]. Ponslet and Steinzig [28] discusses the limitations and assumptions of the hole drilling method. For instance, linear elastic deformation is assumed as well as constant residual stresses parallel to the material surface. Please note that residual stresses close to the yield strength must always be evaluated with caution, as plasticity effects might occur. To correct for such occurring error, Chupakhin et al. [29] proposed a machine learning based correction via a neural network trained via simulation data accounting for plasticity effects. The hole drilling method is used to determine residual stresses up to a depth of 1 mm using a 2 mm diameter drill. In the near-surface area of the specimen, steep gradients of the residual stresses are expected. For this reason, smaller increments at the hole surface than in deeper layer are selected (see Table 3). The residual stress determinations were carried out at five locations along the central line of each specimen, see Fig. 4. Averaged results are reported with its standard deviation in Section 3. The residual stress calculation of the used hole-drilling system PRISM is based on the assumption of an isotropic material behaviour [26]. However, the produced LPBF samples show a slight anisotropy of less than 10% as will discussed later. In this regard, considering the overall experimental scatter of the hole drilling experiments, the influence of the simplification of isotropic material behaviour is assumed to be negligible.

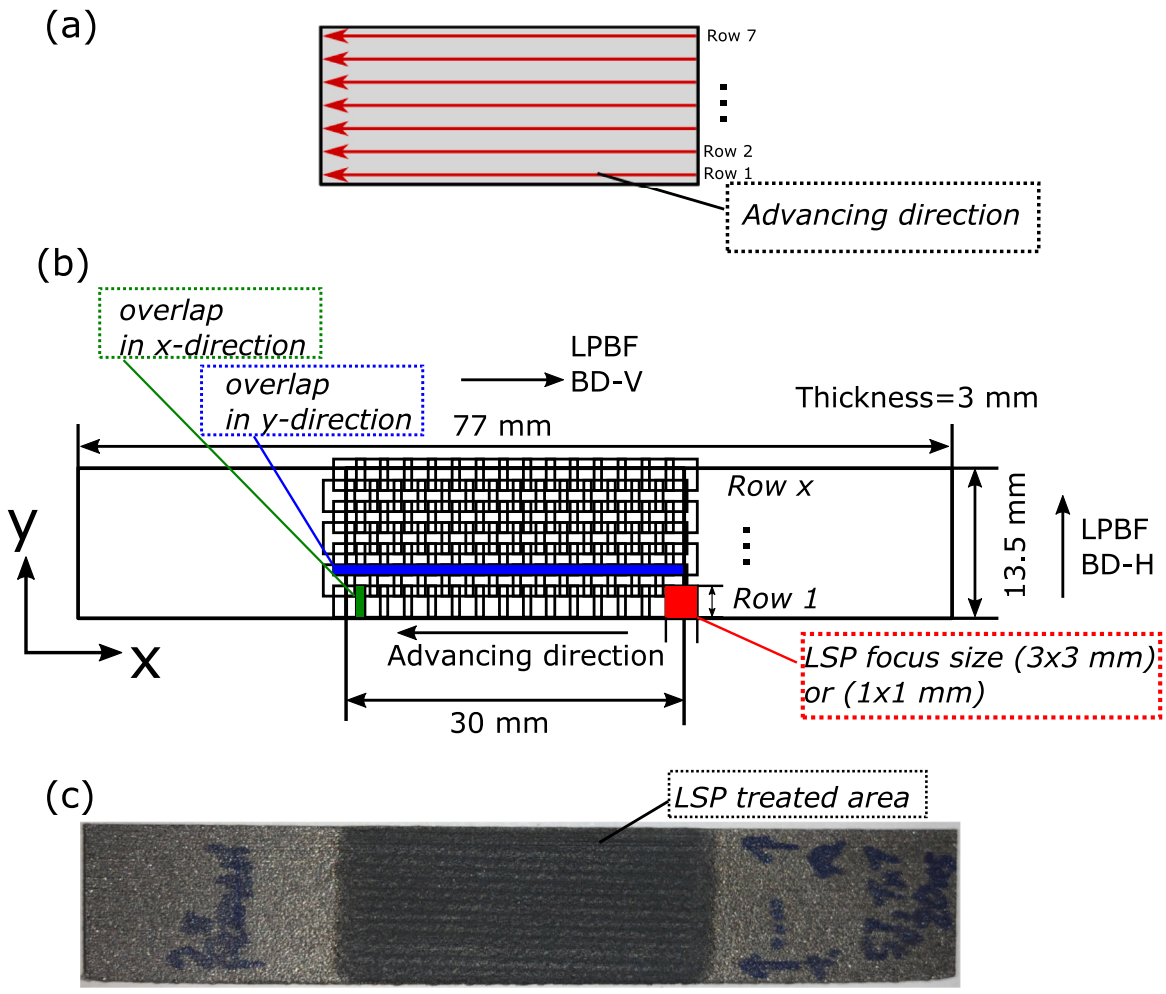

Fig. 3. Illustration of the LSP treatment pattern (a), schematic of LSP treatment pattern (b) and photograph of LPBF 316L specimen processed with LSP (specimen peened with a focus size of 1 mm × 1 mm shown here for illustration) in the middle section (c). LPBF BD-V and LPBF BD-H illustrates the building direction during the manufacturing by LPBF for the vertical and horizontal sample respectively. The LSP advancing direction is perpendicular to the LPBF build direction for the vertical samples (LPBF BD-V) and parallel to the LSP advancing direction for the horizontal samples (LPBF BD-V). The coordinate system is defined in relation to the sample.

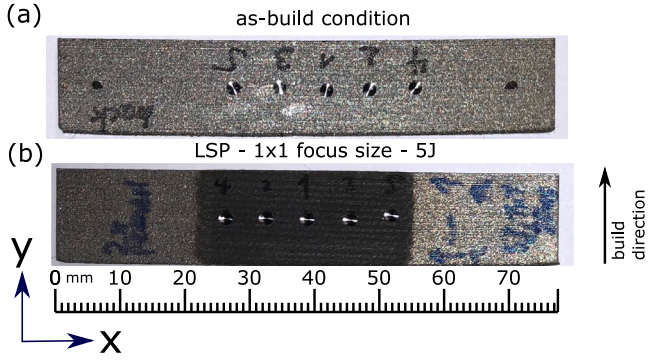

Fig. 4. Illustration of the drill sequence and location for (a) the as-build condition and (b) after LSP with a focus size of 1 mm × 1 mm and a pulse energy of 5 J.

2.5. Tensile tests at elevated temperatures

Tensile tests for LPBF 316L were conducted at room temperature as well as at elevated deformation temperatures to obtain plastic deformation properties at a range of temperatures using a Mayes 200kN tensile rig with attached furnace. The chemical composition of the powder, scan pattern and all other LPBF parameters were already detailed in Section 2.1. The tensile specimen were machined using electrical discharge machining (EDM) and the surface was polished. The 77 mm long tensile dogbone shaped specimens were prepared with a gauge length of 20.5 mm, gauge width of 6 mm as well as a thickness of 2 mm. During the heat-up and testing phases, a thermocouple was attached to the tensile specimens to precisely set the temperature. Two specimens were tested at each temperature to ensure the repeatability of the testing set-up and printed material. The results of the repeated tests were in agreement, i.e. a deviation of less than 5% was noticed. The load–displacement data was recorded and converted into true stress–strain data using the standard equations for a simple tensile test. Subsequently, the true plastic flow stress–strain data is calculated by subtracting the elastic strain from the total strain to estimate the constitutive model parameter in Section 4.1.

3. Results and discussion: Experimentally determined residual stresses

3.1. As-build condition

Due to the rapid heating in the LPBF process and a rather slow heat conduction, a steep temperature gradient develops throughout the building process within the additively manufactured structure. Elastic compressive strains are induced since the underlying layers inhibit the expansion of the heated layers on the top. When the materials yield

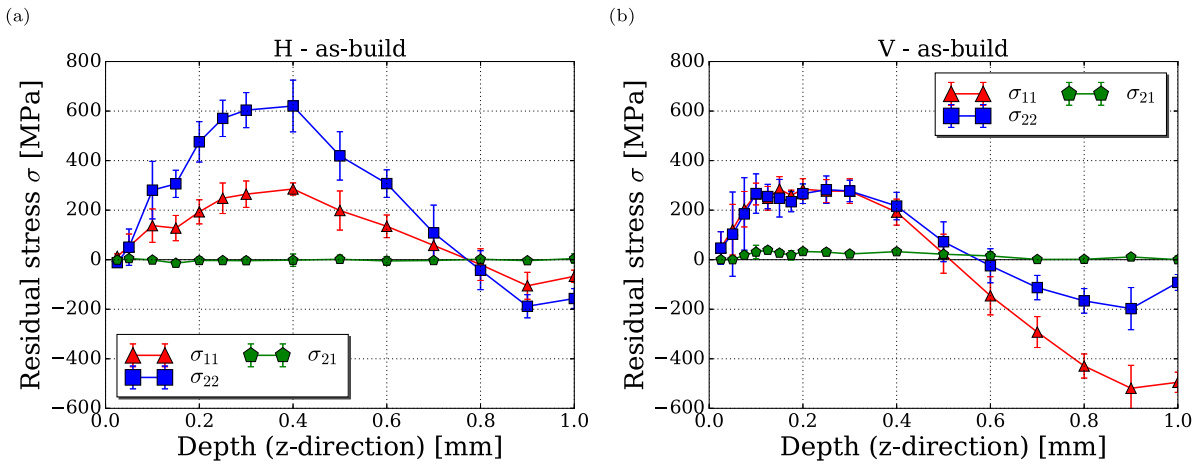

Fig. 5. Determined residual stresses σ_{11}, σ_{22}, σ_{21} using the incremental hole drilling technique. The mean values with its standard deviation are shown for the horizontally (a) and vertically (b) printed specimen in the as-build (AB) condition, see Fig. 1.

strength is reached, which is reduced at elevated temperature, the top layer will be plastically compressed. Upon cooling, the plastically compressed upper layers start to shrink and bend towards the laser beam [30]. Fig. 5 depicts the experimentally obtained residual stresses of samples after being removed from the build plate based on incremental hole drilling in the bar shaped geometry for the horizontally (a) and vertically (b) printed specimens. For the horizontally printed sample, maximum residual stresses close to the yield strength were determined (σ_{22} = 620 ± 90 MPa ; σ_{11} = 280 MPa ± 50 MPa),[1] where the stress component in build direction σ_{22} is higher than the one in the perpendicular direction σ_{11}. The significant lower residual stresses in horizontal direction can be explained by the stress relaxation after the sample removal from the build plate. The as-build residual stresses lead to a relatively large bending deformation due to the small second moment of inertia in the y–z plane, resulting in significant reduction of residual stress σ_{22} in the y-direction. The smaller residual stress level in the vertical sample can be related to the smaller cross-sectional contact area of the build plate, which acts as the primary cooling source of the part via conduction. Therefore more heat is retained in the sample throughout the process leading to a smaller temperature gradient in the build direction of the sample.

3.2. Influence of LSP on the residual stress state in LPBF material

The impact of LSP treatment on the as-build samples (after sectioning the LPBF specimen from the build plate as described in Section 2.1) has been investigated experimentally using two different LSP focus sizes, i.e. 3 mm × 3 mm and 1 mm × 1 mm. Generally, LSP generates compressive residual stresses below the surface of conventional materials from a stress-free initial state. However, in the LPBF samples, the initial stress state in the as-build condition is highly tensile at the surface and compressive at the mid-thickness, see Fig. 5. Nevertheless, LSP was able to convert the original tensile residual stress state into desired compressive residual stresses next to the surface, see Fig. 6. However, the stresses directly at the surface (<0.1 mm) are slightly tensile. Tensile stresses are a common occurrence when performing LSP without a sacrificial overlay [20]. In the mid-thickness of the samples, compressive residual stresses are transformed into tensile residual stresses balancing the change to compressive stresses below the surface. Fig. 6 shows the results of applying identical LSP treatments (3 mm × 3 mm, 5 J) to both sets of printed samples. The results for the horizontal and vertical printed sample after LSP, see Fig. 6(a) and Fig. 6(b), show similar characteristics, however, clear differences due to the initial residual stress state, Fig. 5, are visible. Before applying LSP, the stress state in the horizontal sample is non-biaxial, $|\sigma_{22}| > |\sigma_{11}|$, whereas the stress state for the vertical sample is close to biaxial.

Comparing the residual stresses close to the sample surface (~ 2 mm depth) after applying the same LSP treatment to the horizontal and vertical LPBF 316L sample, it can be observed that for the horizontal sample $|\sigma_{22}| < |\sigma_{11}|$ whereas for the vertical sample $|\sigma_{11}| < |\sigma_{22}|$, comparing Fig. 6(a) and Fig. 6(b). According to LSP studies from Kallien et al. [31] and Keller et al. [32] on conventional stress free material,[2] a high laser power density induces non equi-biaxial residual stresses with a higher compressive stress component perpendicular to the advancing direction (in the present work the y-direction) being present. Due to the advancing direction of the laser detailed in Section 2.2, σ_{22} should, therefore, form higher compressive stresses in conventional stress-free material. This phenomena can also be observed when the LPBF sample has an initial equibiaxial tensile state as observed in the vertical sample (see Fig. 5(b)) leading to a higher compressive stress component σ_{22} sample after applying LSP, see Fig. 6(b). The initial non equi-biaxiality and relatively higher tensile stresses in the σ_{22} component of the LPBF 316L horizontal sample, however, lead to σ_{22} being less compressive after applying LSP.

The phenomenon of the compressive stress component perpendicular to the advancing direction (σ_{22}) being higher after LSP is further amplified by using a smaller laser focus size of 1 mm × 1 mm amounting to a higher laser power density. In addition, this leads to higher experimentally observed compressive residual stresses of up to σ_{11} = −350 MPa and σ_{22} = −300 MPa as well as σ_{11} = −200 MPa and σ_{22} = −400 MPa for the horizontal and vertical sample, respectively, see Fig. 6(c,d).

Applying LSP on the horizontally manufactured LPBF sample twice (sequence overlap) with a focus size of 3 mm × 3 mm (Fig. 7(a)) and 1 mm × 1 mm, Fig. 7(b), leads to a higher magnitude of compressive residual stresses compared to peening only once. In case of the 3 mm × 3 mm focus size the compressive residual stresses where almost doubled for the stress component σ_{22}, see Fig. 6(a) and Fig. 7(a). Peening the sample a second time can therefore further increase the compressive stresses significantly. Further, it can be observed that a sequence overlap (peening twice) leads to a significant reduction in the near tensile surface stresses (at z=0.1 mm) which are present when peening the sample only once.

[1] Note that σ_{11} denotes the residual stress in the x-direction and σ_{22} in the y-direction, respectively.

[2] Rolling also induces residual stresses, however, these stresses are far below the tensile stresses determined in the LPBF material.

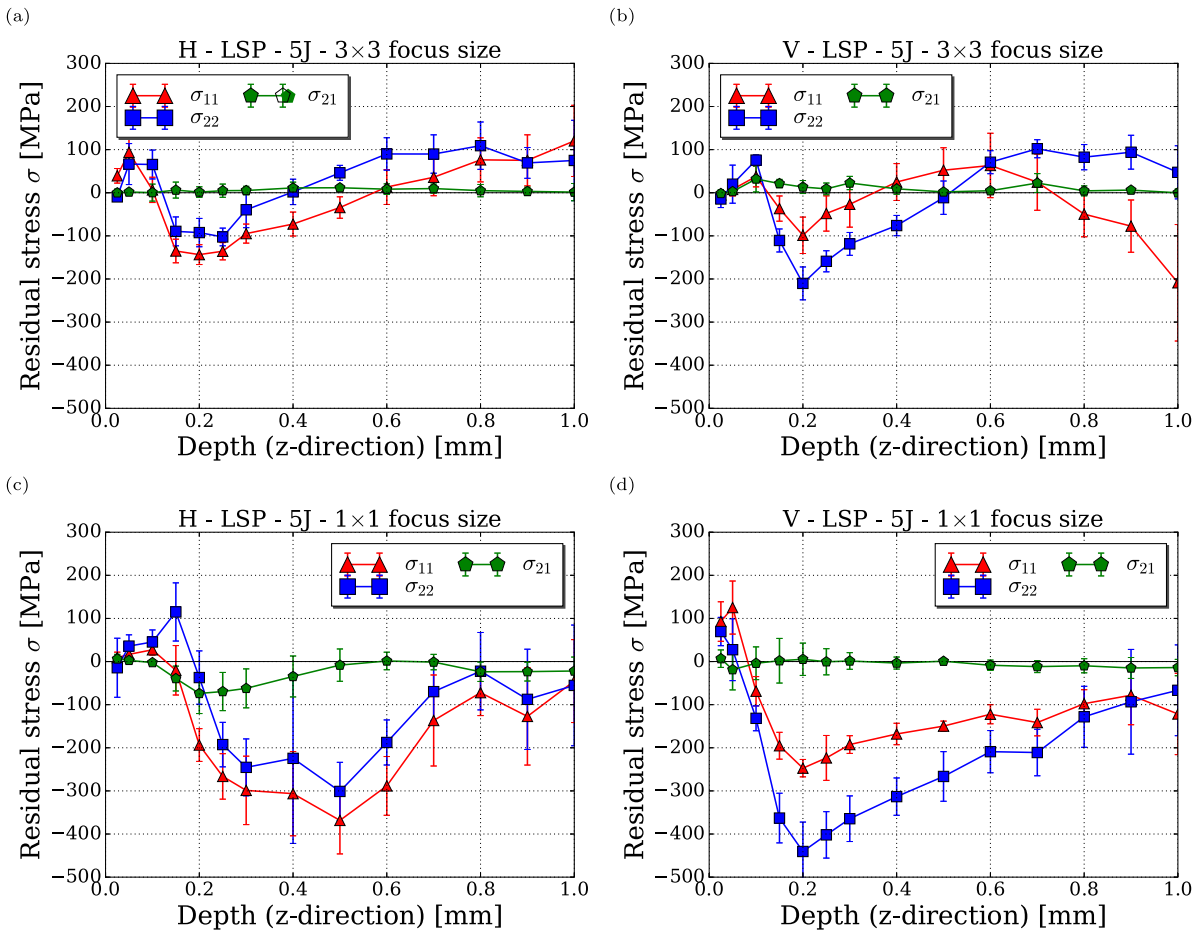

Fig. 6. Influence of LSP on 316L manufactured by LPBF. Shown are the measured residual stresses for LSP (single treatment layer) applied to the horizontally (a,c) and vertically (b,d) printed samples with a focus size of 3 × 3mm (a,b) and 1 × 1mm (c,d).

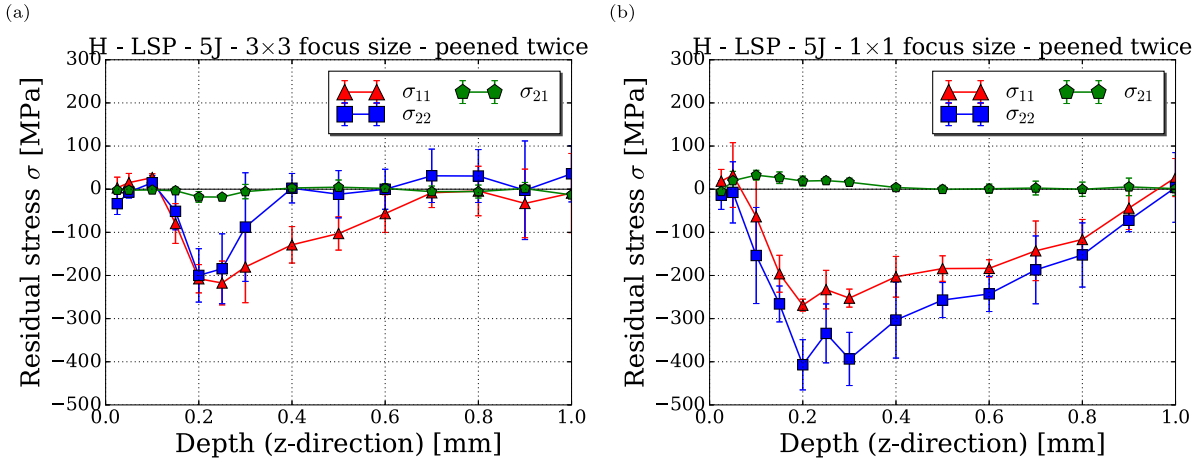

Fig. 7. Influence of LSP sequence overlap on the residual stress state. Shown are residual stress profiles for an LSP sequence peened twice (two LSP treatment layers) with a focus size of 3 × 3mm (a) and 1 × 1mm (b).

3.3. Influence of post-build heat treatment

Heat treatment of the horizontal LPBF sample, Fig. 8(a), at 700 °C for 6 h leads to an overall stress relieve to around half of the as-build condition. However, still, significant stresses are present with maximum tensile stresses of 280 MPa and 135 MPa for the σ_{22} and σ_{11} stress components respectively. The initial stress level had a great impact on the amount of creep deformation and therefore, stress relaxation taking place. It can be observed that the stress component σ_{22} is reduced more than σ_{11} in absolute terms, since the initial residual stress (as-build condition) σ_{22} in y-direction (build direction) is higher than the stress component σ_{11} in x-direction (maximum tensile stress of 420 MPa and 170 MPa, respectively). Further, it can be observed, that the location of the peak tensile stress (~0.2–0.4 mm below the surface) and the peak compressive stress (~0.9–1 mm below the surface) does not change significantly. Heat treatment of the vertical printed sample (comparing

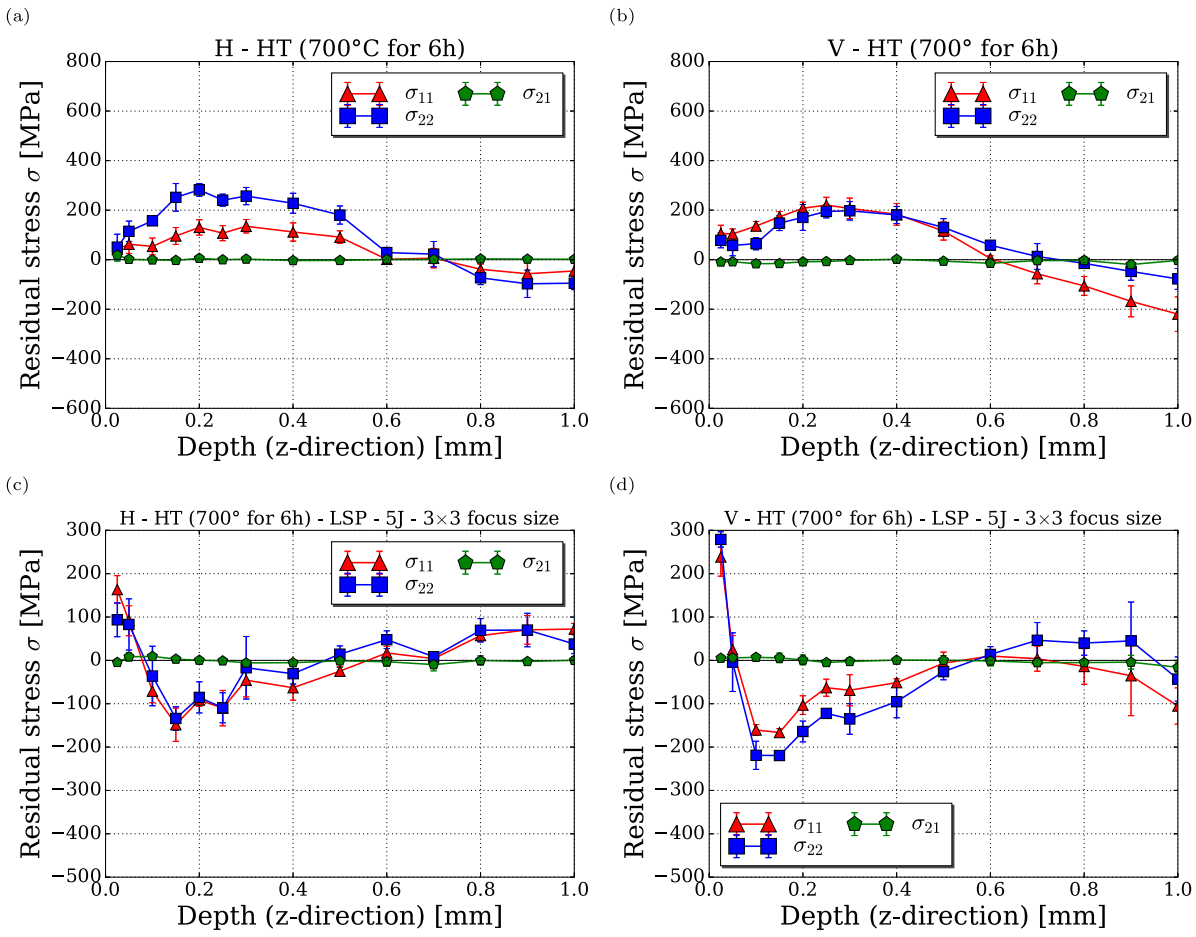

Fig. 8. Influence of post-build heat treatment. Residual stress profiles of samples after heat treatment (a,b) and after heat treatment following subsequent LSP (c,d). This comparison is shown for samples manufactured in the horizontal (a,c) and vertical (b,d) direction.

Fig. 5(b) to Fig. 8(b)) also reduced the residual stresses although the residual stress reduction resulting from the heat treatment was less compared to the horizontal sample amounting to a reduction of only around 30%.

Fig. 8(c) shows the results after heat treatment as well as subsequently employing LSP. Interestingly, an equi-biaxial stress state is formed. The heat treatment reduces the residual stresses so that the residual stress state before applying the LSP is lower compared to the as-build state. Hence, the effect of the initial tensile stresses from LPBF is less pronounced, and therefore an equi-biaxial stress state is more likely to occur.

4. Process simulations

A three-step simulation approach is proposed, enabling the prediction of the residual stresses in as-build 316L samples manufactured by LPBF, after heat treatment and after LSP. Step 1 represents the LPBF process simulation to determine the initial (as-build) residual stress state. Subsequently, the post-build heat treatment is simulated in Step 2. Step 3 describes the LSP process simulation, based on the initial residual stress state obtained from Step 1 or Step 2. The multi-step simulation approach is illustrated in Fig. 9, where the individual steps are described in the following.

4.1. Constitutive modelling and parameter identification

The application of an appropriate constitutive material model is essential for each process simulation. To describe the material behaviour during the LPBF and LSP process, the constitutive model has to be able to account for various deformation temperatures and strain rates. A very successful model for this context represents the Johnson–Cook model, which has already been widely applied in additive manufacturing and LSP simulation. Promoppatum and Rollett [33] compared different plasticity models and found the Johnson–Cook model to accurately capture the plastic material response for a thermomechanical simulation in LPBF. For LSP Amarchinta et al. [34] has compared the Johnson–Cook, Zerilli–Armstrong and an elastic-perfectly plastic model and showed that the Johnson–Cook model consistently match the experimental LSP results.

The Johnson-Cook model [35] considers the effects of strain hardening, strain rate (viscosity) and thermal softening in separate terms and determines the yield stress σ_y by

$$\sigma_y = [A + B\,\varepsilon_P^n]\left[1 + C\,ln\left(\frac{\dot{\varepsilon}_P}{\dot{\varepsilon}_{P,0}}\right)\right]\left[1 - \frac{T - T_0}{T_{melt} - T_0}^{m}\right] \quad (1)$$

where ε_P is the equivalent plastic strain, $\dot{\varepsilon}_P$ is the equivalent plastic strain rate. T is the current temperature, and the melting temperature is defined as T_{melt} (around 1400 °C in the present steel). $\dot{\varepsilon}_{P,0}$ is the reference strain rate and T_0 the reference temperature at which the material constant A (static yield stress), B (strain hardening coefficient), n (strain hardening exponent), C (strain rate hardening parameter), m (thermal softening coefficient) are determined.

Identification of the (J–C) model constants is essential to accurately describe the material deformation behaviour at various deformation temperatures and strain rates. The static yield stress A is defined as the point of non-linearity in the stress–strain curve and determined to be 530 MPa for the vertical sample and 545 MPa for the horizontal printed

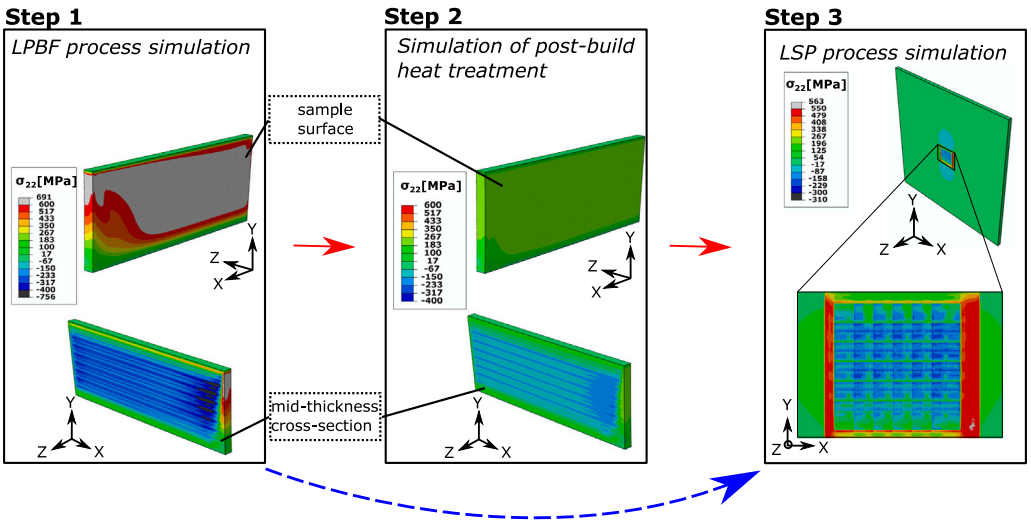

Fig. 9. Multi-step simulation used to determine the residual stresses of materials manufactured by LPBF after LSP. Step 1 represents the LPBF process simulation to determine the residual stress state in the additively manufactured 316L followed by the simulation of the heat treatment (Step 2). Subsequently the extracted residual stresses from Step 1 or 2 are imported into the LSP process simulation as an initial stress state (Step 3). For Step 1/2 only a quarter of the sample is modelled according to the symmetry of the problem, see Section 4.2. The contour plot shown in Step 3 reflects the results after applying LSP directly after the LPBF process simulation (blue dashed arrow).

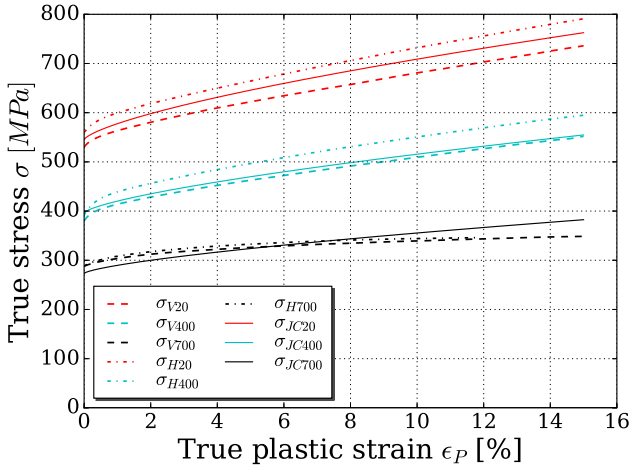

Fig. 10. The measured stress strain curves of LPBF 316L under quasi static tension (4×10^{-4} 1/s) and the curves fitted using the J–C hardening model. The J–C constants fitted to the experimental data are summarized in Table 4. "V" (vertical) and "H" (horizontal) in the variables implies the printing direction of the sample whereas the following number determines the temperature at which the samples were tested. The variable names that include "JC" are the fitted stress–strain curves.

sample from the performed tensile tests, see Fig. 10. The Levenberg–Marquardt nonlinear least square technique [36] is employed to fit the J–C constitutive equation to the experimental tensile stress–strain data. Previously this technique has been used in other studies such as determining the J–C parameters for Ti-6Al-4V as shown by Milani et al. [37] or for two different steels by Sedighi et al. [38]. First, the constants B and n were determined at the reference deformation temperature (T_0=20 °C) and reference strain rate (4×10^{-4} 1/s). To find the thermal softening coefficient m, the fit of Eq. (1) to all experimental data containing vertical and horizontal assuming isotropic material properties. The obtained J–C constants are summarized in Table 4 and the resulting stress–strain curves at different temperatures are shown in Fig. 10(b) for the identified thermal softening coefficient m. The strain rate sensitivity parameter C was taken from literature for conventional 316L (C=0.01) [39].

Norton's law constitutive equation is employed to predict the deformation behaviour of the material exhibiting time-dependent, inelastic deformation at high temperature during the stress relieving heat treatment of the LPBF component. Under steady state condition (constant stress and temperature), the creep strain rate $\dot{\epsilon}_{cr}$ for a power-law creeping material is modelled as

$$\dot{\epsilon}_{cr} = A_{cr}\sigma^{n_{cr}} \tag{2}$$

where σ is the equivalent stress. A_{cr} and n_{cr} represent the power-law creep stress constant and exponent, respectively, and were taken from Williams et al. [40] at 650 °C (see Table 5). However at 700 °C, the creep strain rates are expected to be slightly higher compared to 650 °C, which could lead to a slight over-prediction of the residual stresses in the heat treated samples.

4.2. LPBF and heat treatment

A thermo-mechanical three-dimensional finite element (FE) model was set-up using ABAQUS/Standard [41] to predict the residual stress distribution after the LPBF process. Fig. 11 shows the model for the horizontal (a) and vertical (b) build directions, due to symmetry of the problem only a quarter is explicitly modelled. For the mesh discretization 8-node thermally coupled brick elements with reduced integration (C3D8RT) were used. A uniform element size of 0.15 mm in all direction is used to mesh the specimen. Convergence tests were conducted using different mesh sizes to guarantee a mesh independent solution. To simulate the additive nature of the LPBF process, multiple physical layers in the LPBF process are agglomerated simultaneously on top of each other at the melting temperature (1400 °C) using the element reactivation technique by Williams et al. [12]. For computational efficiency, layers 0.3 mm in thickness were deposited at once representing 6 physical layers (considering the 50 µm layer thickness used in the experimental LPBF setup). By varying the model layer thickness, it was ensured that an independent solution is reached. Since this model does not account for a specific scanning strategy, the process is assumed to be symmetric along the x–y, and y–z planes as well as symmetric along the x–y, and x–z planes for the horizontal and vertical specimen respectively, as depicted in Fig. 11. Therefore, the fully build-in symmetry boundary conditions are applied for both specimens to the respective symmetry surfaces, see Fig. 11(a). The bottom of the specimens (denoted as the side where layers start to be deposited) are fully constrained to account for the part connected to the baseplate

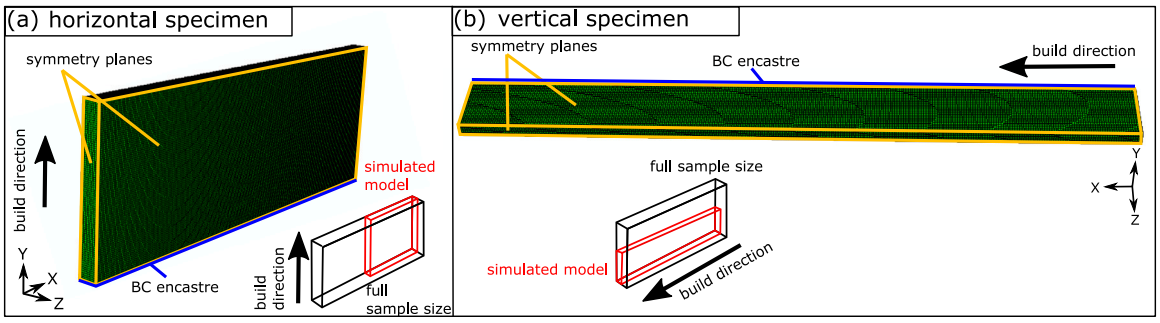

Fig. 11. Three-dimensional FE model used for the simulation of the LPBF process (horizontal specimen (a); vertical specimen (b)). For both building direction only a quarter of the geometry is simulated using symmetry boundary condition.

Table 4
Johnson-Cook model parameters determined for LPBF 316L. The material constants were determined by tensile tests shown in Fig. 10.

Static yield stress, A [MPa]	Strain hardening coefficient, B [MPa]	Strain hardening exponent, n [MPa]	Thermal softening coefficient, m	Melting temperature, T_{melt} [°C]	Reference temperature, T_0 [°C]
545	821	0.7	1.038	1400	20

Table 5
Creep properties for LPBF 316L expressed in terms of Norton's law constitutive equation, taken from [40].

Power-law creep stress coefficient, A_{cr} [h^{-1} MPa^{-1}]	Power-law creep stress exponent, n_{cr}
2.4×10^{-17}	5.71

(see Fig. 11). Sectioning of the part from the baseplate is subsequently simulated by removing this boundary condition.[3]

In terms of heat transfer, a temperature boundary condition was applied to the bottom of the sample, reflecting the temperature of the build plate in the experiment. Subsequently, in the cooling step, the temperature boundary condition is changed to 20 °C to account for the cooling process of the component to ambient temperature. In case of post-build heat treatment, an additional viscoelastic step is added after the baseplate boundary condition is removed in the LPBF process simulation to simulate the time-dependent material behaviour. The thermal expansion coefficient, as well as the conductivity and Young's modulus, have been taken from Williams et al. [12]. Note that the above-mentioned material properties are have been measured for conventional 316L. However, they are not expected to deviate significantly.

4.3. LSP

To simulate the residual stresses after LSP treating additively manufactured components, a multi-step simulation strategy is used, see Fig. 9. Therefore, the residual stress state from the LPBF simulation is imported into the LSP process model as a predefined field. Subsequently, the laser pulse is modelled as a uniform square pressure loading acting to the surface of the specimen, as shown first by Peyre et al. [42] and described in detail in Keller et al. [32]. The maximum pressure pulse applied is approximated by a saw tooth profile, where pressure pulse duration of 2×10^{-7} s and time of maximum pressure of 2×10^{-9} s are taken from Keller et al. [32]. For the used laser system Keller et al. [32] showed that a maximum pressure pulse of $p_{max} = 1350\,\mathrm{N/mm^2}$ led to a very good agreement of the simulation with the experimental results of the hole drilling method for AA2198-T3. As shown via plasma simulation in Pozdnyakov et al. [43] applying identical LSP pulse parameter to aluminium or steel leads to an approximately 10% lower maximum pressure compared to aluminium. This can be explained by the lower energy absorption for steel compared to aluminium. Therefore, the maximum pressure for the simulation was selected 10% lower ($p_{max} = 1215\,\mathrm{N/mm^2}$) compared to Keller et al. [32].

Similar to the experimental LSP setup, 30% overlap between each consecutive pressure pulse is applied as illustrated in Fig. 12(b). For the LSP process simulation, only 6 × 6 laser pulses were simulated, see Fig. 12(b). The principle of periodicity is assumed, i.e. the centre region is representative in terms of the resulting residual stress profile as no further applied peening patch would affect the results of this region further. Therefore, significant computation time can be saved as not the entire LSP pattern, as applied in the experiment, needs to be simulation, see also Keller et al. [44]. In this regard, the LSP simulation consists of 36 dynamic shockwave propagation steps followed by a static relaxation step. Fixed boundary were applied to the sides of the model, see Fig. 12(a), where the model is dimensioned sufficiently large to result in sample size independent results. Initial numerical studies indicate no dependency of calculated residual stresses and peening patch size as well as specimen size for the sample and peening patch size selected.

The minimal element size on the surface was set to 0.1 × 0.1 × 0.04 mm to achieve mesh independence. The material properties of the employed Johnson-Cook model were kept identical to the ones used in the LPBF simulation, see Section 4.1. To compare the residual stresses obtained from experiments, a comparable averaging volume needs to be defined in the FE model similar to Brockman et al. [45]. For the experiment multiple measurements at locations with similar residual stress expectations are averaged, while in the FE simulation an average of a cylindrical volume equivalent to the drilling diameter in the centre of the sample was used (error bars are min and max values of the cylindrical averaging volume shifted to each side by 1.5 mm), see Fig. 13. This assumption is supported by findings of Braisted and Brockman [46] showing the pressure pulse is constant in space over the applied area.

4.4. Results and discussion LPBF and heat treatment

The spatially averaged simulated (σ_{Sim}) and experimentally determined (σ_{HD}) residual stresses using the incremental hole drilling

[3] Rigid body motion are prevented by keeping one point fixed to ensure that the system is statically indeterminate.

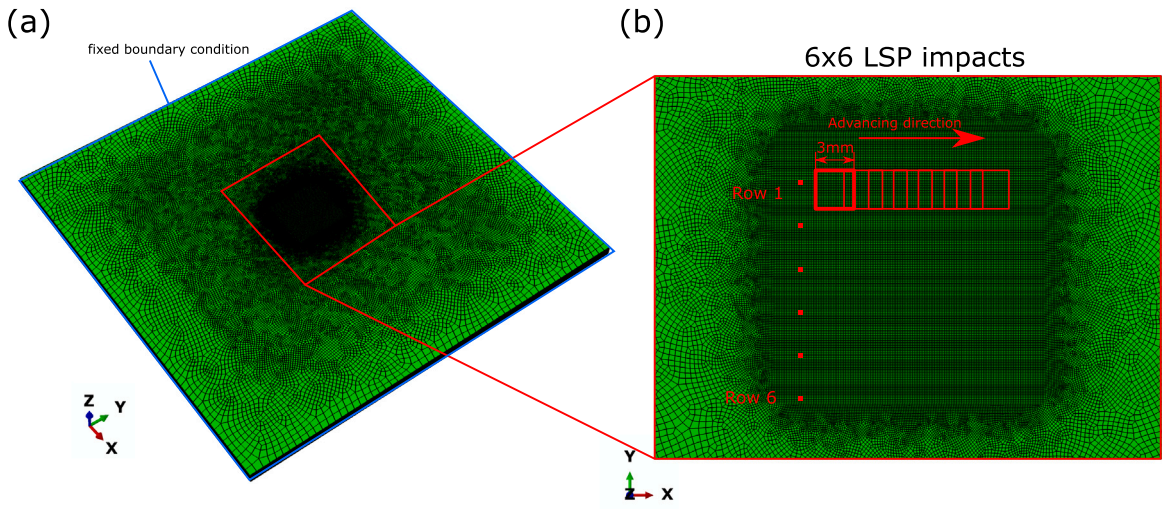

Fig. 12. Three-dimensional FE model used for the simulation of the LSP process (a) and a close-up of the mesh where the LSP impacts are applied to (b).

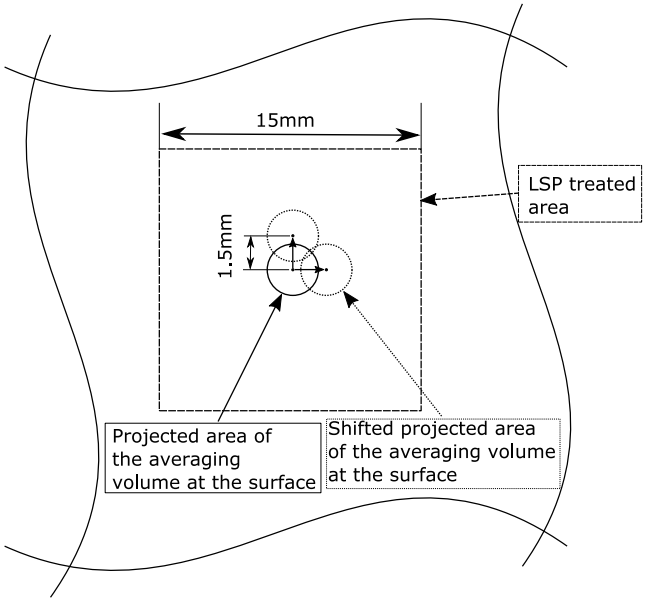

Fig. 13. Schematic detailing the averaging of the residual stresses in the FE simulation in order to compare them to the experimental results. In the FE simulation an averaging volume in the centre of the sample equivalent to the drilling diameter in the experiment is selected. For the error bars, a min and max value of the cylindrical averaging volume shifted from the centre is chosen.

technique are shown in Fig. 14 for the as-build condition (a,b) as well as the residual stress state after heat treatment (6 h at 700 °C) (c,d). Measured and simulated residual stresses are generally in good agreement for both states, showing large tensile residual stresses on surface balanced by compressive stresses next to mid-thickness. While the maximum residual stresses in the build direction (σ_{22} =~600 MPa) for the horizontal as-build condition match very well, see Fig. 14(a), the residual stresses perpendicular to the build direction (σ_{11}) are slightly underestimated by the simulation. One possible reason is expected to be the boundary condition used for simulating the build plate which assumes an infinitely stiff base plate. In the actual LPBF process, the base plate tends to bend slightly. The experimental results for the vertical as-build condition, see Fig. 14(b), indicate an equiaxial stress state. However, for the vertical as-build condition, the σ_{22} component is slightly underestimated by the simulation whereas both simulation and experiment indicate maximum tensile stresses of around 300 MPa for the σ_{11} component. The agreement between the experimentally determined and simulated residual stresses after the heat treatment of the as-build component is also good for both the vertical and horizontally printed specimen, see Fig. 14(c,d), where the simulated values are within the standard deviation of the experimental experiments. Again, the depth up to which tensile residual stresses are observed is in good accordance, and both simulation and experiment illustrate that only the magnitude of the residual stresses decrease by the heat treatment. Sprengel et al. [47] analysed the residual stresses in a cuboidal SEN B specimen via neutron diffraction with the longest axis in the build direction similar to the vertical specimen investigated in the present study. The residual stress distribution reported in the study is in coherent with the data measured in the present study showing tensile residual stresses close to the surface, compressive in the core of the material and an overall reduction by applying a heat treatment. The determined residual stresses reported in Sprengel et al. [47] are comparable with −290 MPa and 220 MPa for the maximum compressive and tensile stresses respectively in the as-build condition. This is slightly lower than the values measured in the present study, however, the specimen is significantly thicker (13 mm vs 3 mm) which is known to have an impact on the residual stresses. Sprengel et al. [47] also investigated the effect of the post-build heat treatment 450° for 4 h and 1 h at 800° showing a reduction for the residual stresses of almost no reduction and 75% respectively. The heat treatment carried out in the present paper with 6 h at 700° reduces the residual stresses by 35% and hence is coherent with the data published to date but cannot be compared directly.

Overall, the simulation correctly predicts the maximum tensile residual stresses at the same depth as observed experimentally as well as the depth of the change from tensile to compressive residual stresses. The simulation and the experimental determined residual stresses are in good accordance, serving as a valid basis for subsequent input to the LSP process simulation.

4.5. Results and discussion LSP

Fig. 15(a,b) shows the comparison between the simulated (σ_{Sim}) and experimentally determined (σ_{HD}) residual stresses after LSP with a pulse energy of 5J and a laser focus size of 3 × 3 for the horizontal and vertical build sample. Overall the experimental and simulated results agree well. Especially, the stress gradient towards the depth of 1 mm is predicted particularly well by the simulation for the σ_{11}. The tensile residual stress close to the surface caused by thermal effects in the LSP process between 0 and 0.2 mm, i.e. partial surface remelting due to the fact that no coating was applied [48], could not be predicted

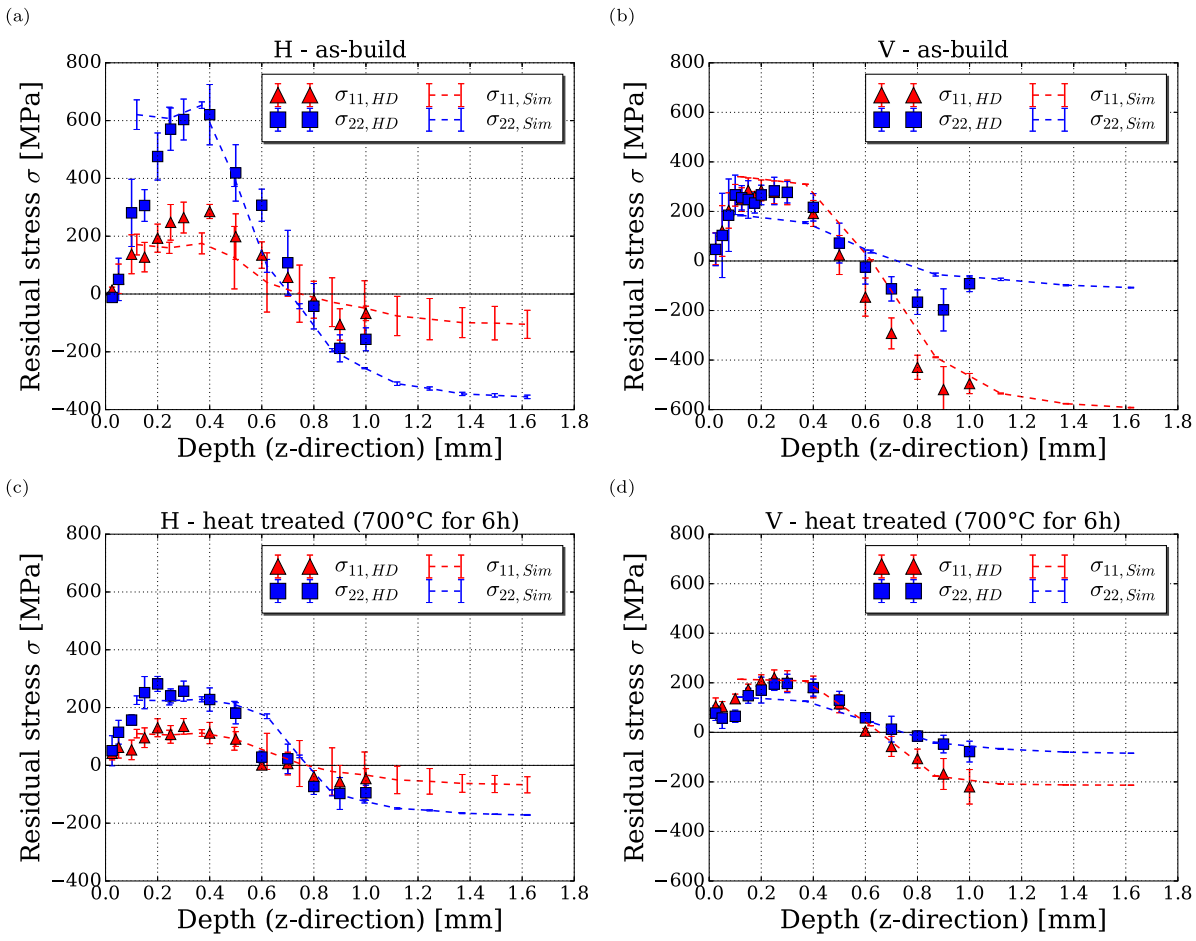

Fig. 14. Comparison between simulated (σ_{Sim}) and experimentally determined (σ_{HD}) residual stresses: in the as-build state (after cutting the specimen from the build plate) (a,b), after heat treating the sample (c,d) for the horizontal (a,c) and vertical (b,d) build samples. The mean values with its standard deviation are shown. For hole drilling multiple measurements at locations with similar residual stresses expectations are averaged, while in the FE simulation nodal stresses are averaged in an area where the hole drilling analysis was conducted.

accurately due to the purely mechanical simulation approach for the LSP process. However, this discrepancy is limited to the near-surface region.[4] Such tensile residual stresses could be removed by applying a protective coating during the LSP experiments [49].

In addition, the results are in accordance with the data published by Busi et al. [50] on 3D LSP where samples are also treated during the building process. Busi et al. [50] investigated the influence of 1 J and 1.5 J with a spot overlap of 40% and 80% and showed that LSP could convert the tensile residual stresses into compressive stresses close to the surface.

As shown in the experiment as well as simulation, the initial stress state in the as-build condition is highly tensile at the surface, see Fig. 14(a,b). Nevertheless, LSP is able to convert the original tensile residual stress state into desired compressive residual stresses below the surface, which is very well reflected in the simulation results. Before LSP, the stress state in the horizontal samples is non-biaxial with the σ_{22} component being higher than the σ_{11} component. However the vertical sample is relatively equibiaxial (see Section 4.4), where the vertical sample showed a nearly equibiaxial stress state. This phenomena can also be observed in LPBF material where the initial state is approximately biaxial for the vertical build direction (see Fig. 14(b)) leading to non equibiaxial residual stress profiles with $|\sigma_{22}| > |\sigma_{11}|$ after LSP, see Fig. 15(b). However, in non-biaxial initial residual stress states as the case for the horizontally printed sample (see Fig. 14(a)), the initially higher tensile residual stress state has an impact on the stress state after LSP. Generally, higher initial tensile stresses lead to less compressive residual stresses after LSP. Accordingly, in the initial state the tensile stress σ_{22} is higher for the horizontal sample, see Fig. 14(a,b), leading to compressive residual stresses σ_{22} with lower magnitude after LSP than for the vertical, see Fig. 15(a,b).

Fig. 15(c,d) shows the residual stresses after applying LSP to the heat treated horizontally and vertically printed sample. The simulation could not capture the biaxiality measured via hole drilling in the horizontal sample and has predicted that stress state of the σ_{11} component is more compressive than σ_{22}, see Fig. 15(c). For the vertical specimen, see Fig. 15(d), the experimental results indicated that the stress component σ_{22} is smaller than σ_{11} ($\sigma_{11} > \sigma_{22}$), which is not correctly predicted by the simulations. Nevertheless, the simulation captured that difference in compressive stress magnitude between σ_{11} and σ_{22} by applying the heat treatment before LSP (comparing Fig. 15(a,b) with Fig. 15(c,d)). Still overall, the simulation was able to predict the general trend as well as the magnitude of the residual stresses.

When peening the horizontal specimen twice, compressive residual stresses are increased in both experiment and simulation (see Fig. 15(e)) and the residual stress profile is less non equibiaxial in comparison with peening only once (see Fig. 15(a)). This is suspected to be attributed to the particular peening advancing direction leading

[4] Although these near-surface tensile residual stresses exists, it has been shown that LSP without coating still has a very beneficial effect on the fatigue crack propagation behaviour, since the propagation behaviour is mainly influenced by the residual stresses deep within the material, see e.g. [32].

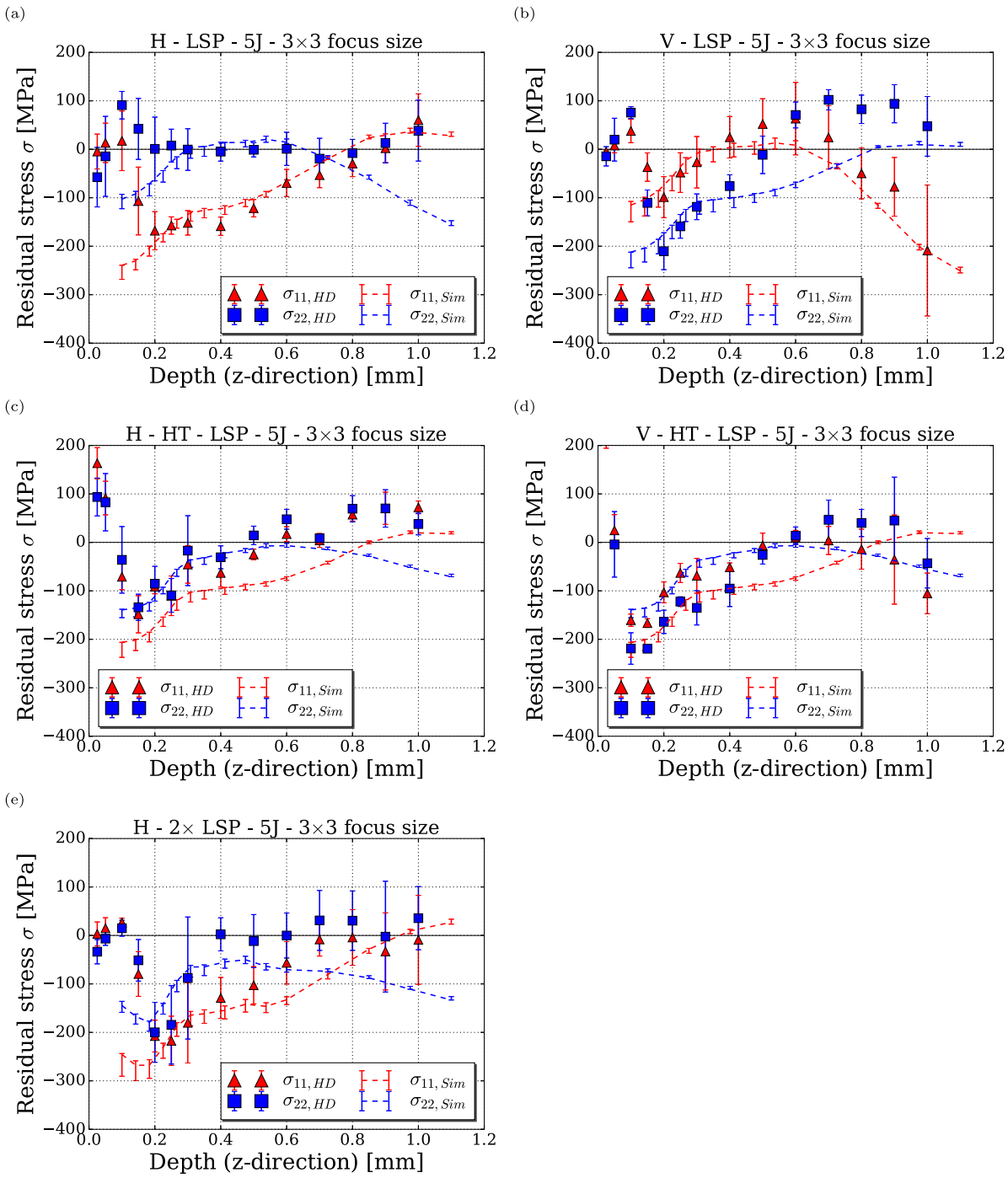

Fig. 15. Comparison between simulated (σ_{Sim}) and experimentally determined (σ_{HD}) residual stresses: after laser shock peening (single LSP layer treatment) a horizontally (a) and a vertically printed sample (b) with pulse energy of 5J and a laser focus size of 3 × 3 mm; after heat treating and subsequent LSP (5J,3 × 3 mm) for the horizontal (c) and vertical (d) sample and after two LSP treatment layers of the horizontal sample (e). For hole drilling multiple measurements at locations with similar residual stresses expectations are averaged, while in the FE simulation a spherical averaging volume within the drilling diameter in the centre of the sample was used (error bars are min and max values of spherical averaging volume shifted from the centre of the sample).

to the stress component perpendicular to it showing increased compressive residual stresses (in the present work σ_{22}). Also in the simulation, the difference in residual stresses between the σ_{11} and σ_{22} component shrinks and thus predicting this phenomenon correctly.

5. Summary and conclusion

The influence of LSP on residual stresses in LPBF 316L has been investigated with an experimental and multi-step simulation approach. To quantify the residual stresses experimentally, the incremental hole drilling technique was used. The initial residual stress for an vertical and horizontal cuboid shaped bar manufactured via LPBF were determined. Further, the influence of LSP in general, sequence overlap and post-build heat treatment on as-build LPBF material has been investigated experimentally. A sequential FE simulation strategy is applied to be able to predict the residual stresses caused by LSP on the LPBF material containing high initial tensile stresses near the surface. In a first step a thermo-mechanical simulation of the selective laser melting process is performed to predict the initial residual stress state in the LPBF material. If applied, an additional heat treatment process is

simulation. The next step includes the transfer of the residual stresses onto a simplified smaller component geometry using a predefined field approach. Afterwards, a dynamic LSP process simulation was used. Overall, LSP has demonstrated to be a promising local modification technique to induce beneficial compressive residual stresses for LPBF parts with their initial high tensile residual stress below the surface. The main conclusions can be summarized as follows:

- Simulated and measured residual stress profiles are in good agreement for both, the as-build condition (after removing the specimen from the build plate), treatment as well as after LSP. The LSP simulation has proven to be valuable in predicting the residual stresses after laser shock peening as well as heat treatment of LPBF components by importing the residual stress results from the experimentally validated LPBF simulation before or after heat treatment.
- Consistent with residual stress analysis published to date, tensile residual stresses are found at the surface balanced by compressive residual stresses deeper in the LPBF material. The orientation of the component on the build plate plays a major role with regard to residual stress development. Mostly two factors are influencing the residual stress development in this regard. First, the height versus contact area to build plate ratio is relevant as this determines the thermal gradient. The higher the component is in the build direction the lower the thermal gradient is and therefore the resulting residual stress. When removing the sample from the build plate, the second moment of area of component plays a major role since this determines the deflection and stress relaxation.
- Heat treating the as-build LPBF sample at 700 °C for 6 h showed not to be effective in eliminating all tensile residual stresses present. However, an overall reduction of residual stress magnitude (compressive as well as tensile) with no change in peak position to around a third of the as-build condition was observed.
- LSP is able to convert the initial detrimental tensile residual stresses into desired compressive residual stresses in the near surface region which are balanced by tensile residual stresses in deeper layers. The magnitude of the initial tensile residual stresses has an impact on the stress field generated by LSP.
- LSP has a different effect of on the stress components parallel to the surface depending on the laser pulse sequence, e.g. LSP advancing direction. This can be utilized to compensate for or purposely taylor the non-equibiaxial initial stress fields as present in LPFB material.

CRediT authorship contribution statement

Paul Sandmann: Conceptualization, Validation, Formal analysis, Investigation, Data curation, Writing – original draft, Writing – review & editing, Visualization, Project administration. **Sören Keller:** Conceptualization, Methodology, Validation, Writing – review & editing. **Nikolai Kashaev:** Resources, Writing – review & editing, Funding acquisition. **Shaaz Ghouse:** Resources. **Paul A. Hooper:** Resources, Supervision. **Benjamin Klusemann:** Conceptualization, Methodology, Resources, Writing – review & editing, Funding acquisition. **Catrin M. Davies:** Conceptualization, Methodology, Resources, Writing – review & editing, Supervision, Project administration, Funding acquisition.

Declaration of competing interest

The authors declare that they have no known competing financial interests or personal relationships that could have appeared to influence the work reported in this paper.

Data availability

Data will be made available on request.

Acknowledgement

BK and NK acknowledge the funding by the Deutsche Forschungsgemeinschaft (DFG, German Research Foundation) - project number 459713992.

References

[1] C. Li, J. Liu, Y. Guo, Prediction of residual stress and part distortion in selective laser melting, Proc. CIRP 45 (2016) 171–174.
[2] J.-P. Kruth, G. Levy, F. Klocke, T. Childs, Consolidation phenomena in laser and powder-bed based layered manufacturing, CIRP Ann. 56 (2007) 730–759.
[3] Z. Snow, A.R. Nassar, E.W. Reutzel, Invited review article: Review of the formation and impact of flaws in powder bed fusion additive manufacturing, Addit. Manuf. 36 (2020) 101457.
[4] R.J. Williams, F. Vecchiato, J. Kelleher, M.R. Wenman, P.A. Hooper, C.M. Davies, Effects of heat treatment on residual stresses in the laser powder bed fusion of 316l stainless steel: Finite element predictions and neutron diffraction measurements, J. Manuf. Process. 57 (2020) 641–653.
[5] D. Gu, W. Meiners, K. Wissenbach, R. Poprawe, Laser additive manufacturing of metallic components: Materials, processes and mechanisms, Int. Mater. Rev. 57 (2012) 133–164.
[6] A. Dunbar, E. Denlinger, J. Heigel, P. Michaleris, P. Guerrier, R. Martukanitz, T. Simpson, Development of experimental method for in situ distortion and temperature measurements during the laser powder bed fusion additive manufacturing process, Addit. Manuf. 12 (2016) 25–30.
[7] R. McClung, A literature survey on the stability and significance of residual stresses during fatigue, Fatigue Fract. Eng. Mater. Struct. 30 (2007) 173–205.
[8] Renishaw, Design for Metal Am - A Beginner's Guide, 2020, URL https://resources.renishaw.com/en/details/--101490.
[9] C. Li, J. Liu, X. Fang, Y. Guo, Efficient predictive model of part distortion and residual stress in selective laser melting, Addit. Manuf. 17 (2017) 157–168.
[10] A. Hussein, L. Hao, C. Yan, R. Everson, Finite element simulation of the temperature and stress fields in single layers built without-support in selective laser melting, Mater. Des. (1980-2015) 52 (2013) 638–647.
[11] L. Parry, I. Ashcroft, R.D. Wildman, Understanding the effect of laser scan strategy on residual stress in selective laser melting through thermo-mechanical simulation, Addit. Manuf. 12 (2016) 1–15.
[12] R.J. Williams, C.M. Davies, P.A. Hooper, A pragmatic part scale model for residual stress and distortion prediction in powder bed fusion, Addit. Manuf. 22 (2018) 416–425.
[13] M. Shiomi, K. Osakada, K. Nakamura, T. Yamashita, F. Abe, Residual stress within metallic model made by selective laser melting process, CIRP Ann. 53 (2004) 195–198.
[14] N. Kalentics, E. Boillat, P. Peyre, S. Ćirić-Kostić, N. Bogojević, R.E. Logé, Tailoring residual stress profile of selective laser melted parts by laser shock peening, Addit. Manuf. 16 (2017) 90–97.
[15] N. Kalentics, M.O.V. de Seijas, S. Griffiths, C. Leinenbach, R.E. Loge, 3D laser shock peening–A new method for improving fatigue properties of selective laser melted parts, Addit. Manuf. 33 (2020) 101112.
[16] N. Kalentics, A. Burn, M. Cloots, R.E. Logé, 3D laser shock peening as a way to improve geometrical accuracy in selective laser melting, Int. J. Adv. Manuf. Technol. 101 (2019) 1247–1254.
[17] N. Kalentics, N. Sohrabi, H.G. Tabasi, S. Griffiths, J. Jhabvala, C. Leinenbach, A. Burn, R.E. Loge, Healing cracks in selective laser melting by 3D laser shock peening, Addit. Manuf. 30 (2019) 100881.
[18] H. Zhang, Z. Cai, J. Chi, R. Sun, Z. Che, H. Zhang, W. Guo, Fatigue crack growth in residual stress fields of laser shock peened Ti6Al4v titanium alloy, J. Alloys Compd. 887 (2021) 161427.
[19] L. Hackel, J.R. Rankin, A. Rubenchik, W.E. King, M. Matthews, Laser peening: A tool for additive manufacturing post-processing, Addit. Manuf. 24 (2018) 67–75.
[20] P. Peyre, R. Fabbro, Laser shock processing: A review of the physics and applications, Opt. Quantum Electron. 27 (1995) 1213–1229.
[21] Renishaw, Data sheet SS316L-0407 powder for additive manufacturing, 2019, URL https://www.renishaw.com/media/pdf/en/f8cba72a843440d3bd8a09fd5021ad89.pdf.
[22] K. Ding, L. Ye, Laser Shock Peening: Performance and Process Simulation, Woodhead Publishing, 2006.
[23] M. Montero Sistiaga, S. Nardone, C. Hautfenne, J. Van Humbeeck, Effect of heat treatment of 316l stainless steel produced by selective laser melting (SLM), in: Proceedings of the 27th Annual International Solid Freeform Fabrication Symposium-an Additive Manufacturing Conference, 2016, pp. 558–565.
[24] T. Ronneberg, C.M. Davies, P.A. Hooper, Revealing relationships between porosity, microstructure and mechanical properties of laser powder bed fusion 316l stainless steel through heat treatment, Mater. Des. 189 (2020) 108481.
[25] G.S. Schajer, Advances in hole-drilling residual stress measurements, Exp. Mech. 50 (2010) 159–168.
[26] M. Steinzig, E. Ponslet, Residual stress measurement using the hole drilling method and laser speckle interferometry: Part 1, Exp. Tech. 27 (2003) 43–46.

[27] E. Ponslet, M. Steinzig, Residual stress measurement using the hole drilling method and laser speckle interferometry. Part II: Analysis technique, Exp. Tech. 27 (2003) 17–21.
[28] E. Ponslet, M. Steinzig, Residual stress measurement using the hole drilling method and laser speckle interferometry Part III: Analysis technique, Exp. Tech. 27 (2003) 45–48.
[29] S. Chupakhin, N. Kashaev, B. Klusemann, N. Huber, Artificial neural network for correction of effects of plasticity in equibiaxial residual stress profiles measured by hole drilling, J. Strain Anal. Eng. Des. 52 (2017) 137–151.
[30] P. Mercelis, J.-P. Kruth, Residual stresses in selective laser sintering and selective laser melting, Rapid Prototyp. J. 12 (2006) 254–265.
[31] Z. Kallien, S. Keller, V. Ventzke, N. Kashaev, B. Klusemann, Effect of laser peening process parameters and sequences on residual stress profiles, Metals 9 (2019) 655.
[32] S. Keller, S. Chupakhin, P. Staron, E. Maawad, N. Kashaev, B. Klusemann, Experimental and numerical investigation of residual stresses in laser shock peened AA2198, J. Mater Process. Technol. 255 (2018) 294–307.
[33] P. Promoppatum, A.D. Rollett, Physics-based and phenomenological plasticity models for thermomechanical simulation in laser powder bed fusion additive manufacturing: A comprehensive numerical comparison, Mater. Des. 204 (2021) 109658.
[34] H. Amarchinta, R. Grandhi, K. Langer, D. Stargel, Material model validation for laser shock peening process simulation, Modelling Simulation Mater. Sci. Eng. 17 (2008) 015010.
[35] G.R. Johnson, A constitutive model and data for materials subjected to large strains, high strain rates, and high temperatures, in: Proc. 7th Inf. Sympo. Ballistics, 1983, pp. 541–547.
[36] K. Levenberg, A method for the solution of certain non-linear problems in least squares, Quart. Appl. Math. 2 (1944) 164–168.
[37] A. Milani, W. Dabboussi, J.A. Nemes, R. Abeyaratne, An improved multi-objective identification of Johnson–Cook material parameters, Int. J. Impact Eng. 36 (2009) 294–302.
[38] M. Sedighi, M. Khandaei, H. Shokrollahi, An approach in parametric identification of high strain rate constitutive model using hopkinson pressure bar test results, Mater. Sci. Eng. A 527 (2010) 3521–3528.
[39] H. Chandrasekaran, R. M'saoubi, H. Chazal, Modelling of material flow stress in chip formation process from orthogonal milling and split Hopkinson bar tests, Mach. Sci. Technol. 9 (2005) 131–145.
[40] R.J. Williams, J. Al-Lami, P.A. Hooper, M.-S. Pham, C.M. Davies, Creep deformation and failure properties of 316l stainless steel manufactured by laser powder bed fusion under multiaxial loading conditions, Addit. Manuf. 37 (2021) 101706.
[41] A.S.U. Manual, Abaqus 6.11, 89, 2012, p. v6, http://130.149.
[42] P. Peyre, I. Chaieb, C. Braham, Fem calculation of residual stresses induced by laser shock processing in stainless steels, Modelling Simulation Mater. Sci. Eng. 15 (2007) 205.
[43] V. Pozdnyakov, S. Keller, N. Kashaev, B. Klusemann, J. Oberrath, Coupled modeling approach for laser shock peening of AA2198-T3: From plasma and shock wave simulation to residual stress prediction, Metals 12 (2022) 107.
[44] S. Keller, M. Horstmann, N. Kashaev, B. Klusemann, Experimentally validated multi-step simulation strategy to predict the fatigue crack propagation rate in residual stress fields after laser shock peening, Int. J. Fatigue 124 (2019) 265–276.
[45] R.A. Brockman, W.R. Braisted, S.E. Olson, R.D. Tenaglia, A.H. Clauer, K. Langer, M.J. Shepard, Prediction and characterization of residual stresses from laser shock peening, Int. J. Fatigue 36 (2012) 96–108.
[46] W. Braisted, R. Brockman, Finite element simulation of laser shock peening, Int. J. Fatigue 21 (1999) 719–724.
[47] M. Sprengel, A. Ulbricht, A. Evans, A. Kromm, K. Sommer, T. Werner, J. Kelleher, G. Bruno, T. Kannengiesser, Towards the optimization of post-laser powder bed fusion stress-relieve treatments of stainless steel 316l, Metall. Mater. Trans. A 52 (2021) 5342–5356.
[48] J. Kaufman, J. Racek, M. Cieslar, P. Minárik, M.A. Steiner, S.R. Mannava, V.K. Vasudevan, A. Sharma, M. Böhm, J. Brajer, et al., The effect of laser shock peening with and without protective coating on intergranular corrosion of sensitized AA5083, Corros. Sci. 194 (2022) 109925.
[49] R. Fabbro, P. Peyre, L. Berthe, X. Scherpereel, Physics and applications of laser-shock processing, J. Laser Appl. 10 (1998) 265–279.
[50] M. Busi, N. Kalentics, M. Morgano, S. Griffiths, A.S. Tremsin, T. Shinohara, R. Logé, C. Leinenbach, M. Strobl, A parametric neutron bragg edge imaging study of additively manufactured samples treated by laser shock peening, Sci. Rep. 11 (2021) 1–9.